Charge-Transport Parameters of Acenedithiophene Crystals: Realization of One-, Two-, or Three-Dimensional Transport Channels through Alkyl and Phenyl Derivatizations

ARTICLE *in* THE JOURNAL OF PHYSICAL CHEMISTRY C · FEBRUARY 2012

Impact Factor: 4.77 · DOI: 10.1021/jp210778w

3 AUTHORS, INCLUDING:

Yuanping Yi
Chinese Academy of Sciences
82 PUBLICATIONS **1,571** CITATIONS
SEE PROFILE

Lingyun Zhu
National Center for Nanoscience and Technol…
42 PUBLICATIONS **541** CITATIONS
SEE PROFILE

THE JOURNAL OF PHYSICAL CHEMISTRY C

Article

pubs.acs.org/JPCC

Charge-Transport Parameters of Acenedithiophene Crystals: Realization of One-, Two-, or Three-Dimensional Transport Channels through Alkyl and Phenyl Derivatizations

Yuanping Yi, Lingyun Zhu, and Jean-Luc Brédas*,†

School of Chemistry and Biochemistry and Center for Organic Photonics and Electronics, Georgia Institute of Technology, Atlanta, Georgia 30332-0400, United States

Supporting Information

ABSTRACT: The charge-transport parameters in a series of naphthodithiophene (NDT) and anthradithiophene (ADT) derivatives are investigated by means of density functional theory and molecular dynamics calculations. In the case of unsubstituted and alkylated NDT and ADT crystals, the results point to small effective masses for the charge carriers along either essentially one dimension (π-stacks) or two dimensions (within the molecular layers), i.e., where large electronic couplings or band widths are present. Interestingly, diphenyl substitutions can lead to small effective masses for both holes and electrons along the three dimensions. This implies that one-, two-, or three-dimensional charge-transport mechanisms can be realized in the alkyl and phenyl NDT and ADT crystals. In particular, the smallest effective mass (and, as a result, the largest expected charge-carrier mobility) is obtained in the diphenyl NDT and ADT crystals along the direction perpendicular to the herringbone molecular layers. Our calculations also point to large nonlocal vibrational couplings along the π-stacks in the unsubstituted and dimethylated ADT crystals.

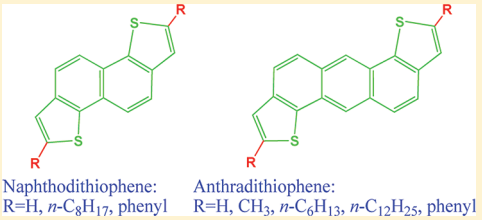

1. INTRODUCTION

π-Conjugated materials have attracted considerable attention due to their potential applications in (opto)electronic devices such as organic field-effect transistors,[1−3] light-emitting diodes,[4−6] or solar cells.[7−9] Heteroacenes, such as linear acenedithiophenes and their derivatives,[10−22] are of particular interest since these compounds can display hole mobilities similar to that in pentacene and, at the same time, provide enhanced oxidative stability. In contrast to the widely investigated linear acenedithiophenes and their derivatives, only few studies have been conducted on their analogues with a "bent" geometry.

Recently, Takimiya and co-workers have synthesized a bent naphthodithiophene (NDT) and its dioctyl and diphenyl derivatives, see Figure 1, and managed to obtain single-crystal

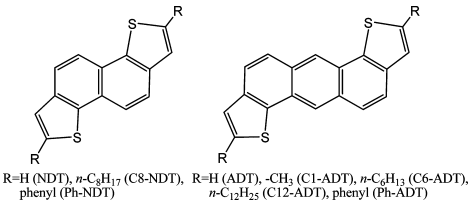

Figure 1. Chemical structures of NDT and ADT and their derivatives studied in this work.

structures.[22,23] Thin-film field-effect transistors were fabricated by using the dioctyl and diphenyl derivatives as the active components. While solution-processed devices based on dioctyl NDT demonstrated no field effect due to the poor quality of the films on Si/SiO_2 substrates, diphenyl NDT-based devices fabricated via vapor deposition on the same substrates displayed relative high hole mobilities (~0.3 $cm^2\ V^{-1}\ s^{-1}$).[22,23] The more extended bent anthradithiophene (ADT) molecule and its derivatives functionalized with alkyl chains of various lengths or with phenyl groups, see Figure 1, have been synthesized by Pietrangelo et al.[24,25] Single-crystal X-ray analysis revealed very different molecular packing modes for these compounds. The unsubstituted and dialkylated ADTs adopt a slipped cofacial stacking arrangement with varying displacements along their long and short molecular axes, while diphenyl ADT packs in a herringbone structure.[24,25] To the best of our knowledge, the charge-transport properties of these ADT derivatives have been characterized neither experimentally nor theoretically.

As is well established, the charge-transport parameters depend on both the molecular electronic properties and the intermolecular packing arrangements in the solid state. In this work, we seek to establish structure-transport properties relationships among these NDT and ADT derivatives by evaluating the electronic structure and charge-transport parameters at both molecular and crystal levels. This analysis is done by means of density functional theory and molecular dynamics calculations.

Received: November 9, 2011
Revised: January 11, 2012
Published: February 1, 2012

   dx.doi.org/10.1021/jp210778w | J. Phys. Chem. C 2012, 116, 5215−5224

2. THEORETICAL METHODOLOGY

The molecular geometries of the neutral, radical-cation, and radical-anion states were optimized by density functional theory (DFT) with the B3LYP functional[26,27] and the 6-31G(d,p) basis set,[28−30] as implemented in the *Gaussian 09* program.[31] The ionization potentials, electron affinities, and reorganization energies were calculated at the same level of theory from the relevant points on the potential energy surfaces.

The crystal structures were optimized with the cell parameters fixed at the experimental values. The electronic band structure and density of states (DOS) were then calculated using both the optimized and experimental crystal structures; these calculations were performed at the DFT-B3LYP/6-31G(d) level with the CRYSTAL06 package.[32] Uniform k-point meshes were employed in the Monkhorst-Pack scheme[33] as follows: 4 × 12 × 12 for NDT, 15 × 6 × 6 for C8-NDT, 12 × 9 × 3 for Ph-NDT, 4 × 12 × 4 for ADT, 6 × 8 × 4 for C1-ADT, 6 × 8 × 2 for C6-ADT, 10 × 8 × 2 for C12-ADT, and 2 × 6 × 8 for Ph-ADT. The inverse effective mass tensor was calculated from the band structure by using Sperling's centered difference method with dk = 0.01 Bohr^{-1}. Subsequent diagonalization of m_{ij}^{-1} provides the principal components and their orientations.

The thermal fluctuations of the transfer integrals were derived by combining molecular dynamics (MD) simulations and quantum-chemical calculations. To prevent artificial symmetry effects, the supercells were initially created via replication of the unit cells according to the following size: 4 × 5 × 4 for NDT, 5 × 8 × 4 for C8-NDT, 6 × 4 × 5 for Ph-NDT, 5 × 6 × 5 for ADT, C1-ADT, and C6-ADT, 6 × 6 × 5 for C12-ADT, and 5 × 6 × 6 for C12-ADT. The MD simulations were carried out with the Discover module of the Materials Studio package using the COMPASS force field.[34] Each system was equilibrated for 150 ps using an Anderson thermostat in the NVT ensemble at 298 K and a time step of 1 fs. After equilibration, a simulation of 150 ps was run and 5000 frames were extracted by taking a snapshot every 30 fs along the trajectory.

The transfer integrals for the molecular pairs taken from the MD simulation snapshots and the DFT-optimized crystal structures were evaluated by using a fragment orbital approach[35] in combination with a basis set orthogonalization procedure.[36] These calculations were performed at the DFT-B3LYP/6-31G(d,p) level with the *Gaussian 09* package.[31]

3. RESULTS AND DISCUSSIONS

3.1. Molecular Properties. Ionization Potentials and Electron Affinities. The calculated ionization potentials (IP) and electron affinities (EA) are given in Table 1. The adiabatic IP is 7.10 eV for the parent NDT, which is ca. 0.8 eV higher than that for tetracene (6.28 eV) at the same level of theory.[37] The more extended ADT system displays a lower adiabatic IP of 6.62 eV; this value is higher than those for both pentacene (5.90 eV)[37] or the linear anthradithiophene (6.15 eV).[12] Alkylations lead to a decrease of IP by ca. 0.5 and 0.3 eV for NDT and ADT, respectively, due to electron-donating character of the alkyl chains. The decrease in IP due to phenyl substitutions and the more extended conjugation they bring is even larger, ca. 0.7 eV for Ph-NDT and 0.4 eV for Ph-ADT. While the parent and dioctylated NDT molecules present EAs that at our level of theory are calculated to be endothermic, the EAs for the other compounds are exothermic. As expected, phenyl substitutions result in more exothermic EAs; on the other hand, the EAs for the dialkyl derivatives are slightly less exothermic or more endothermic with respect to the parent acenedithiophenes.

Table 1. Vertical and Adiabatic Ionization Potentials and Electron Affinities for the Studied NDT and ADT Derivatives (in eV)[a]

	IP		EA	
	vertical	adiabatic	vertical	adiabatic
NDT	7.23	7.10	0.35	0.24
C8-NDT	6.74	6.62	0.40	0.29
Ph-NDT	6.53	6.41	−0.37	−0.57
ADT	6.68	6.62	−0.31	−0.39
C1-ADT	6.44	6.37	−0.25	−0.33
C6-ADT	6.35	6.28	−0.27	−0.35
C12-ADT	6.34	6.27	−0.27	−0.35
Ph-ADT	6.27	6.19	−0.66	−0.79

[a]Here we define IP = $E(M^+) - E(M)$ and EA = $E(M^-) - E(M)$.

Reorganization Energies. The reorganization energy (λ), which measures the strength of the so-called local electron−phonon coupling,[38] can be decomposed into intra- and intermolecular contributions; the former results from changes in the geometry of individual molecules and the latter, from changes in the polarization of the surrounding molecules upon going from the neutral to the charged state and vice versa. As the contribution from intermolecular polarization is expected to be very small in nonpolar systems,[39,40] here, we focus on the intramolecular contribution to λ. The intramolecular reorganization energy can be calculated from the adiabatic potential energy surfaces of the molecular states involved in the considered charge-transfer process. For instance, the reorganization energy for hole/electron transport (λ_h/λ_e) is estimated as the sum of the relaxation energy in the cationic/anionic state in going from the neutral to the ionic geometry (λ_h^+/λ_e^-) and the relaxation energy in the ground state in going from the ionic to the neutral geometry (λ_h^0/λ_e^0).

The DFT-calculated reorganization energies are collected in Table 2. The λ_h values are 265 and 133 meV for the parent NDT and ADT compounds, respectively; these values are substantially larger than the value calculated for pentacene[41,42] and the linear anthradithiophene[12] (both estimated to be ca. 95 meV) but similar to that for rubrene (159 meV).[43] The λ_e value is 237 meV for NDT and 164 meV for ADT; the latter is close to the λ_e value for the linear anthradithiophene (161 meV)[12] and even smaller than that found in good electron-transporters, such as perfluoropentacene (222 meV)[37] or *N,N′*-dipentyl-

Table 2. Intramolecular Reorganization Energies (in meV) for Holes (λ_h) and Electrons (λ_e) in the Studied NDT and ADT Derivatives

	λ_h^+	λ_h^0	λ_h	λ_e^-	λ_e^0	λ_e
NDT	129	135	265	116	121	237
C8-NDT	122	129	251	109	113	221
Ph-NDT	125	120	245	192	145	338
ADT	67	66	133	82	82	164
C1-ADT	69	69	138	80	80	161
C6-ADT	71	72	143	81	81	161
C12-ADT	71	72	143	80	81	161
Ph-ADT	79	79	158	124	115	239

dx.doi.org/10.1021/jp210778w | J. Phys. Chem. C 2012, 116, 5215−5224

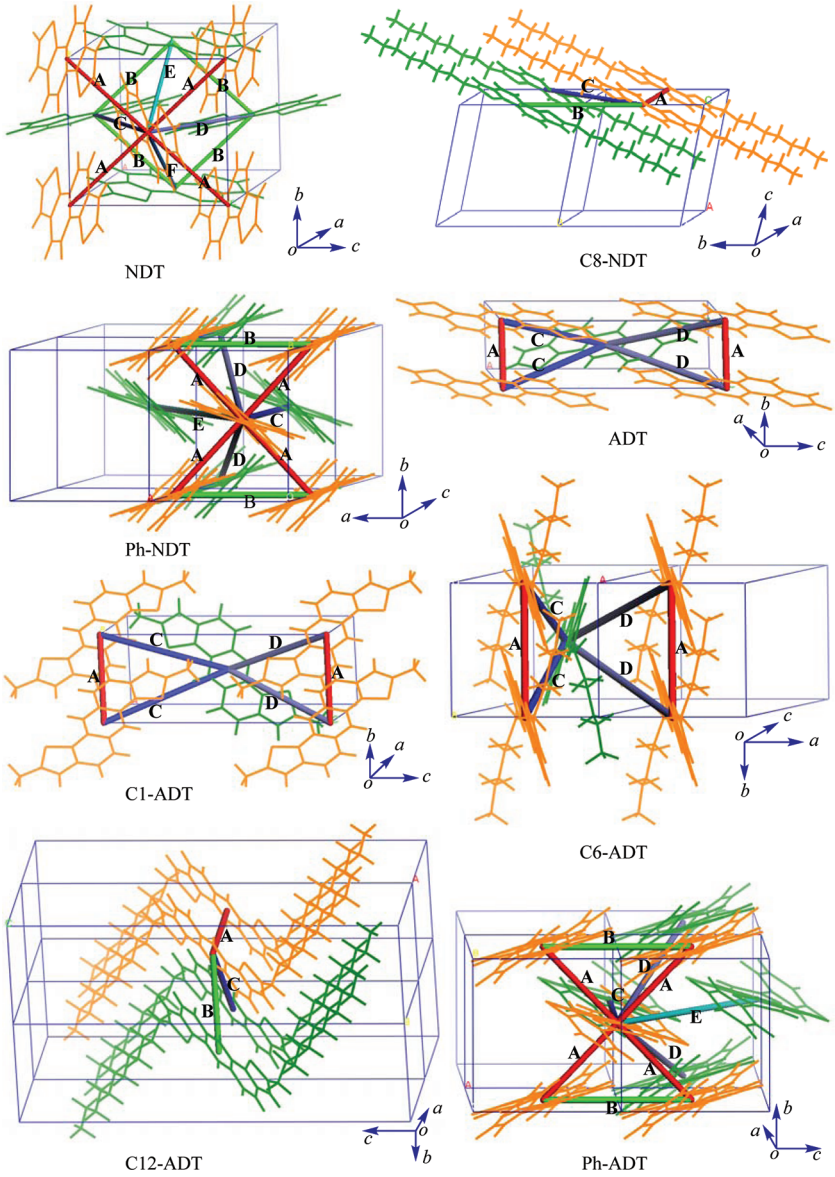

Figure 2. Crystal structures of the NDT and ADT derivatives and illustrations for the nearest neighboring molecular pairs considered in the transfer-integral calculations.

3,4,9,10-perylene tetracarboxylic diimide (272 meV).[44] From NDT to ADT, the substantial decrease in both λ_h and λ_e can be attributed to smaller overall geometric modifications upon charging (see Figure S1). Alkylations result in reorganization energies for both holes and electrons similar to those in the unsubstituted counterparts, due to the similar geometric changes (see Figure S1). In the case of diphenyl NDT and ADT, the geometry relaxations upon ionization reflect the changes in both bond lengths and torsion angles between the central acenedithiophene core and the terminal phenyl groups. In the neutral state, the diphenyl NDT and ADT compounds display the same DFT-optimized torsion angle of 27.2°. Upon oxidation, the torsion angle decreases to 12.6° and 17.1° for the phenyl NDT and phenyl ADT molecules, respectively. Thus, the λ_h values only slightly change upon phenyl substitutions. On the other hand, the diphenyl NDT and ADT compounds relax to a coplanar geometry upon reduction; as a result, the λ_e values significantly increase and reach 338 meV for Ph-NDT and 239 meV for Ph-ADT.

3.2. Crystal Properties. Geometry and Molecular Packing. Table S1 lists the crystallographic parameters for the unit cells of the studied systems.[23−25] The DFT-optimized crystal geometries are shown in Figure 2. The optimized bond lengths agree well with the experimental X-ray diffraction values (the largest differences being within 0.03 Å, see Figure S2). In the case of the diphenyl derivatives, the torsion angles between the central acenedithiophene core and the terminal phenyl groups are slightly overestimated by the DFT calculations (7° for Ph-NDT and 2° for Ph-ADT, see Figure S2) in comparison to the experimental measurements.

We now turn to a discussion the molecular arrangements within the acenedithiophene crystals. C8-NDT and C12-ADT crystallize in the triclinic space group *P*-1, with one molecule per unit cell. The other systems are characterized by a monoclinic space group: *P*21/*c* for NDT and C6-ADT, *P*21/*a* for Ph-NDT and Ph-ADT, and *P*21/*n* for ADT and C1-ADT; there are four molecules per unit cell for NDT and two molecules per unit cell in the other systems. The molecular

dx.doi.org/10.1021/jp210778w | J. Phys. Chem. C 2012, 116, 5215−5224

packing modes for these crystals can be generally classified into two types: herringbone-type and parallel π-stacking.

Unsubstituted NDT presents two kinds of herringbone motif within the *bc* plane, corresponding to two inequivalent molecular layers. The molecular long axis of NDT (in this work, this long axis is defined as the line connecting the two α carbons in the thienyl groups of the acenedithiophene core) displays a substantial tilt angle (ca. 30°) with respect to the direction perpendicular to the herringbone plane (approximately parallel to the *a* direction), which leads to a reduced interlayer distance. In the case of phenyl substitutions, herringbone-like structures are formed in the *ab* and *bc* planes for Ph-NDT and Ph-ADT, respectively. It is interesting to note that, unlike NDT, the molecular long axes of the diphenyl derivatives are almost perpendicular to the herringbone plane, resulting in a maximized interlayer distance.

In contrast, the other systems (including the parent ADT and all the dialkyl NDT and ADT compounds) tend to adopt parallel π-stacking along the shortest crystal axis with varying displacements and interplanar distances; these are listed in Table 3. Although C6-ADT displays the smallest interplanar distance, large short-axis displacements (6.76 Å) result in nearly vanishing spatial overlap between the ADT cores of two neighboring molecules. For the other π-stacks, the interplanar distances are in the range of 3.31−3.72 Å, that is, about twice the van der Waals radii of carbon (1.70 Å); the displacements along the molecular long- and short-axes are rather limited and lead to significant spatial overlaps between two neighboring molecules. Interestingly, in addition to the π-stack along the shortest axis (*a* axis), stacks paralleled to other crystal directions (i.e., *b* axis) are also found for C8-NDT and C12-ADT; in particular, typical two-dimensional molecular layers are formed in the *ab* plane for C12-ADT. It can be anticipated that the variety in molecular arrangements in these crystals will strongly affect the intermolecular parameters, such as transfer integrals and band structures.

Table 3. Displacements (Å) along the Molecular Long- and Short-Axes (d_{long} and d_{short}) and Interplanar Distances (d_{plane}) for the π-Stacks in the Parent ADT and the Dialkyl NDT and ADT Crystals, Corresponding to Pairs Labeled A in Figure 2

	d_{long}	d_{short}	d_{plane}
C8-NDT	0.63	4.08	3.44
ADT	0.79	1.63	3.58
C1-ADT	3.17	3.44	3.31
C6-ADT	0.21	6.76	1.92
C12-ADT	3.71	0.86	3.72

Transfer Integrals. The transfer integrals or electronic couplings play a central role in the understanding of the transport properties in both band and hopping regimes.[45] The calculated transfer integrals for the nearest-neighbor molecular pairs are collected in Table 4; all these molecular pairs are illustrated in Figure 2. Pairs A and B are composed of molecules within the same herringbone-type layer for NDT, Ph-NDT, and Ph-ADT or a parallel π-stack for C8-NDT, ADT, C1-ADT, C6-ADT, and C12-ADT. On the other hand, the molecules in pairs C, D, E, and F belong to adjacent (equivalent or inequivalent) molecular layers or π-stacks. Consequently, electronic couplings for pairs A and B are, in general, larger than those for pairs C, D, E, and F.

All the stacks in the π-stacking systems (pairs A), with the exception of C6-ADT, present significant electronic couplings for both holes and electrons, with the largest value reaching 135 meV for C1-ADT. Compared with C8-NDT, the unsubstituted and dialkyl ADT systems present much more unbalanced electronic couplings for holes and electrons. For instance, the electronic coupling for holes is at least twice smaller than the coupling for electrons in ADT and C1-ADT, whereas the situation is opposite in C12-ADT. For C8-NDT and C12-ADT, strong electronic couplings are found along other parallel-stacking directions, such as for molecular pairs B and C.

Not surprisingly, all the herringbone-type pairs A and B also exhibit significant electronic couplings (except for the relatively small coupling for electrons in Ph-ADT). It is interesting to point out that, for Ph-NDT and Ph-ADT, although the intermolecular distances for the interlayer pairs (C, D, and E)

Table 4. Hole and Electron Transfer Integrals (t_h and t_e, in meV) and Intermolecular Distances (d, in Å) for the Molecular Pairs Taken from the Optimized NDT and ADT Crystals

		NDT	C8-NDT	Ph-NDT	ADT	C1-ADT	C6-ADT	C12-ADT	Ph-ADT
A	t_h	49.2	27.4	26.8	−40.7	−28.4	15.6	109.4	−24.4
	t_e	−61.0	52.4	−38.9	108.9	135.8	5.6	−20.1	−6.4
	d	5.57	5.37	5.02	4.01	5.73	7.03	5.32	5.01
B	t_h	−42.7	−31.1	3.8				35.3	14.8
	t_e	−11.5	6.7	−3.7				17.4	−2.0
	d	5.57	11.12	6.82				6.75	6.98
C	t_h	−5.0	−0.5	5.9	−1.0	15.5	−4.3	0.3	−2.2
	t_e	12.4	33.9	4.4	3.4	−20.1	−7.0	4.7	−2.3
	d	10.11	12.03	19.05	7.79	8.82	11.65	8.00	20.84
D	t_h	14.0		2.8	1.6	11.0	0.0		2.2
	t_e	−15.3		2.5	3.3	−14.5	0.9		1.0
	d	9.66		19.67	10.79	9.61	14.22		21.31
E	t_h	1.1		2.6					−1.0
	t_e	−2.4		−3.3					1.0
	d	9.73		20.19					21.74
F	t_h	−7.8							
	t_e	16.2							
	d	9.73							

dx.doi.org/10.1021/jp210778w | J. Phys. Chem. C 2012, 116, 5215−5224

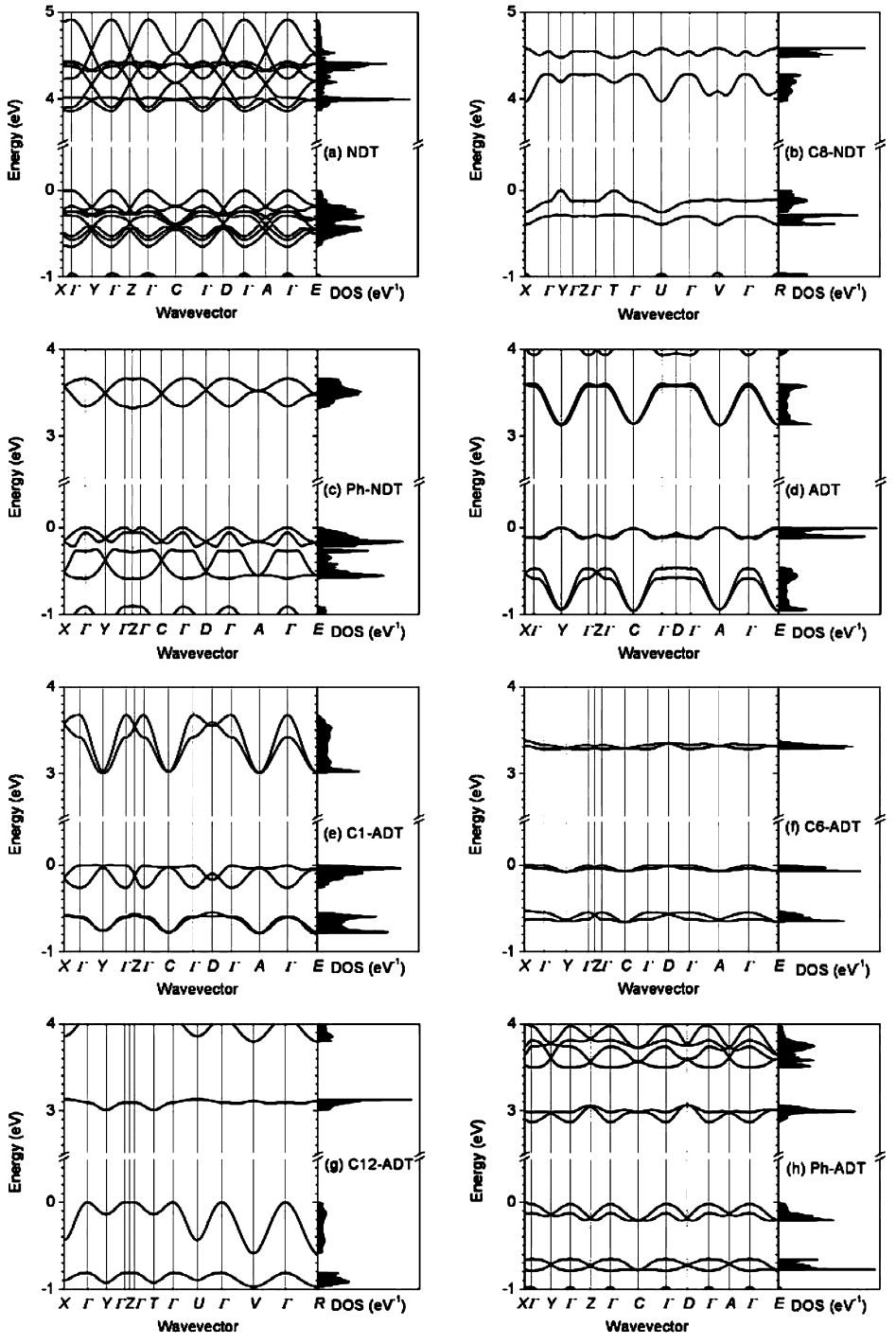

Figure 3. Electronic band structures and density of states for the optimized NDT and ADT crystals. Points of high symmetry in the first Brillouin zone are labeled as follows: Γ = (0,0,0), *X* = (0.5,0,0), *Y* = (0,0.5,0), *Z* = (0,0,0.5), *C* or *T* = (0,0.5,0.5), *D* or *U* = (0.5,0,0.5), *A* or *V* = (0.5,0.5,0), and *E* or *R* = (0.5,0.5,0.5), all in reciprocal lattice vectors (*a**, *b**, and *c**). The Fermi energy is taken as the origin of the energy axis.

are as large as 20 Å (which is nearly four times larger than the intermolecular distances for the intralayer pairs), somewhat significant electronic couplings are calculated for these pairs (on the order of one tenth the couplings for the intralayer pairs). Since our main goal here is to point out the main trends among analogous compounds and not necessarily to provide precise values of charge-carrier mobilities, we base our charge-transport analysis on a hopping mechanism. This assumption appears to be reasonable for Ph-NDT and Ph-ADT since the electronic couplings for all molecular pairs are much (at least 5 times) smaller than the reorganization energies for both holes and electrons. When considering a given direction along two neighboring molecules, the charge-carrier mobility along that direction can be expressed as[46]

$$\mu = \frac{qd^2}{k_B T} k_{ET} \tag{1}$$

where q represents the charge of the carrier; d, the intermolecular distance between adjacent molecules; k_B, the

dx.doi.org/10.1021/jp210778w | J. Phys. Chem. C 2012, 116, 5215−5224

Boltzmann constant; T, the temperature; and k_{ET}, the electron-transfer rate. According to the semiclassical model of Marcus electron-transfer theory, this rate can be described as[47,48]

$$k_{ET} = t^2 \sqrt{\frac{\pi}{\lambda k_B T \hbar^2}} \exp\left[-\frac{(\Delta G + \lambda)^2}{(4\lambda k_B T)}\right] \quad (2)$$

Here t denotes the transfer integral; ΔG, the free energy difference between reactants and products; and $\hbar$, the Planck constant. From eqs 1 and 2, it is seen that the mobility is quadratically proportional to both electronic coupling and intermolecular distance. Considering that there are four times as many channels for interlayer hopping as for intralayer hopping, on the basis of the above model, the mobility along the interlayer direction in Ph-NDT and Ph-ADT could be expected to be at least similar to the intralayer mobility. We will come back to this issue later; at this stage, it is useful to underline that to provide accurate estimates of the charge-carrier mobilities, more complex methodologies, based for instance on a kinetic Monte Carlo approach[49,50] or a master equation approach,[51] should be considered in combination with improved expressions for the hopping rates (that would take into account the relatively strong electronic couplings[52] and incorporate the quantum nature of the nuclear degrees of freedom[53,54]).

Band Structures. The electronic band structures of the studied NDT and ADT crystals are shown in Figure 3. In general, the valence [conduction] band consists of sub-bands arising from the interactions among the monomer HOMO [LUMO] levels. For nondegenerate molecular energy levels, the number of these subbands is equal to the number of inequivalent molecules in the primitive unit cells; this is actually the case for all the studied systems except NDT. In the case of NDT, the molecular HOMO [LUMO] and HOMO-1 [LUMO +1] levels present very small energy differences (in particular, the difference between the highest occupied level energies is smaller than 0.1 eV). Because of strong interactions between the monomer energy levels (large electronic couplings for both holes and electrons, as mentioned above), the HOMO and HOMO-1 [LUMO and LUMO+1] bands appear to cross each other. Even in the case of the functionalized NDT systems (C8-NDT and Ph-NDT), the HOMO band remains very close to the HOMO-1 band with the energy gap between the two bands on the order of thermal energy at room temperature. For ADT, the interaction between the interstack molecules is very weak; as a result, the two sub-bands appear nearly degenerate in both the conduction and valence bands.

The conduction and valence band widths and the band gaps are listed in Table 5. Note that the band widths in the NDT crystal correspond to the total HOMO/HOMO-1 or LUMO/LUMO+1 widths. The ADT, C1-ADT, and C12-ADT crystals exhibit rather unbalanced conduction and valence band widths; ADT and C1-ADT show the largest valence band widths (477 and 666 meV, respectively) and C12-ADT, the largest conduction bandwidth (590 meV). These values are slightly larger than the values that would be derived from a one-dimensional tight-binding model (along the b axis for ADT and C1-ADT, $4t_h$ = 436 and 543 meV, and along the a axis for C12-ADT, $4t_e$ = 438 meV); the more pronounced deviations from a tight-binding model for the C1-ADT and C12-ADT crystals can be attributed to their relatively stronger interstack interactions. Because of its weakest overall electronic couplings, C6-ADT displays the narrowest conduction and valence band widths.

Table 5. Valence (VB) and Conduction (CB) Bandwidths and Band Gaps for the Optimized NDT and ADT Crystals

	VB (meV)	CB (meV)	band gap (eV)
NDT	649[a]	1058[a]	3.857
C8-NDT	255 (120)[b]	322	3.966
Ph-NDT	227 (339)[b]	342	3.320
ADT	128	477	3.126
C1-ADT	262	666	3.009
C6-ADT	80	103	3.278
C12-ADT	590	126	3.005
Ph-ADT	216	204	2.865

[a]The value of VB (CB) reported here is the total width of the HOMO and HOMO-1 (LUMO and LUMO+1) bands. [b]The widths for the HOMO and HOMO-1 bands are both reported (the value in parentheses is the width of the HOMO-1 band).

In general, both dispersive and relatively flat bands appear in all studied systems. This is a reflection of the anisotropic intermolecular interactions occurring in the crystals. In the case of the herringbone-type crystals, the narrow bandwidth in the ΓX direction for NDT and Ph-ADT or in the ΓZ direction for Ph-NDT (which corresponds mainly to the a- or c-axis in direct space) is a clear indication of the weak interlayer interactions. However, as we discussed in the previous section, adjacent molecules along the diagonal directions of the herringbone motif interact strongly and evenly, which translates into similarly large band dispersions in the other directions. In the case of ADT, well-defined one-dimensional π-stacks are present along the b-axis. As a result, flat bands appear in the ΓX and ΓZ directions (which lie in the ac plane in direct space) and strongly dispersive bands are present along the ΓY direction (which corresponds to the b direction in direct space). In addition to strongly dispersive bands in the π-stacking direction, C1-ADT exhibits dispersive bands in the other directions as well, which reflects that substantial intermolecular interactions take place for the interstack pairs. For the C8-NDT and C12-ADT crystals, flat bands appear only in the ΓZ direction; in the other directions, there are two types of bands, reflecting either large or relatively small dispersions. This is consistent with the fact that molecules in these two crystals interact with different strengths along the two parallel-stacking directions. By and large, the band dispersions agree well with the results of the transfer integral calculations on molecular pairs.

Effective Masses. According to band theory, the charge carrier mobility in a wide band is given by[55]

$$\mu = \frac{q\tau}{m} \quad (3)$$

Here τ denotes the mean free time between scattering events (or the mean relaxation time of the band state) and m represents the effective mass of the charge carrier. In the isotropic relaxation time approximation, the mobility and its orientational anisotropy are dictated by the effective mass. In the case of wide bands where the excess holes [electrons] occupy states near the top [bottom] of the valence [conduction] band, the effective mass can be calculated from

the band structures at the band extrema. The inverse effective mass tensor m_{ij}^{-1} for a three-dimensional crystal is defined as[55]

$$\frac{1}{m_{ij}} = \frac{1}{\hbar^2}\frac{\partial^2 E(k)}{\partial k_i \partial k_j} \quad (4)$$

where the subscripts i and j denote the Cartesian coordinates in reciprocal space, $E(k)$ is the band energy, and k the electron wavevector.

The calculated hole and electron effective masses are reported in Table 6. The effective masses display interesting orientational anisotropies. As expected, for the ADT and C1-ADT crystals, the effective masses for electrons are much smaller than those for holes and the smallest values are calculated along the π-stacking direction, 2.08 m_0 for ADT and only 0.92 m_0 for C1-ADT. In the case of the C8-NDT crystal, the smallest effective mass is as low as 0.94 m_0 for holes along the b direction and 0.73 m_0 for electrons approximately along the diagonal direction of the ab plane; these values are about twice as small as the effective mass for holes in pentacene (1.7 m_0).[56] In addition, a rather small effective mass for electrons (3.57 m_0) is also found along approximately the diagonal direction of the ab plane. For the C12-ADT crystal, which is representative of a two-dimensional π-stacking mode, as a result of the combined contributions from different transport channels, two small and more balanced effective masses for holes (1.43 and 2.10 m_0) appear along the ab directions. In the case of the parent NDT crystal, which presents herringbone-type molecular layers in the bc plane, there also exist two relatively small effective masses for both holes and electrons within the bc plane (2.12 and 2.17 m_0 for holes and 1.04 and 3.60 m_0 for electrons). Most interestingly, the phenyl substitutions of NDT and ADT give rise to three small effective masses for both holes and electrons in the range of 1.0−4.3 m_0. In particular, the direction of the smallest effective mass leans toward the interlayer direction (c and a direction for Ph-NDT and Ph-ADT, respectively), although the interlayer electronic couplings are much smaller than the couplings for the intralayer herringbone-type pairs. We note that in the context of solar cells based on the diphenyl acenedithiophenes, these molecules tend to stand on the substrates when vapor deposited.[22,23] Such isotropic charge transport could help charge separation at the donor−acceptor interfaces. To summarize, the studied crystals present one, two, or three directions along which small effective masses are calculated for holes and/or electrons. Thus, through alkyl or phenyl derivatizations, one-, two-, or three-dimensional charge transport can be achieved in the bent acenedithiophene crystals. Due to the fact that structural disorder and defects appear inevitably in devices fabricated in thin-film forms, since there are more pathways for charges in three-dimensional transport systems, the difference in charge carrier mobilities observed between the thin-film transistors based on C8-NDT and Ph-NDT,[22,23] is consistent with the one- or three-dimensional charge-transport characteristics of the respective crystals.

Table 6. Hole and Electron Effective Masses m (in Units of the Electron Mass at Rest, m_0) at the Band Extrema for the Optimized NDT and ADT Crystals

	hole			electron		
	extreme	m/m_0	parallel to	extreme	m/m_0	parallel to
NDT	Γ	2.12	c+0.040a	Γ	1.04	c-0.073a
		2.17	b		3.60	b
		19.4	a-0.060c		9.83	a+0.477c
C8-NDT	Y	0.94	b+0.063a +0.012c	X	0.73	a+0.440b +0.005c
		5.67	a+0.028b +0.030c		3.57	a-0.540b-0.003c
		36.6	c+0.257a +0.354b		27.8	c+0.383a +0.360b
Ph-NDT	Γ	1.02	c+0.602a	Z	1.97	a-0.058c
		4.26	a-0.075c		2.08	c+0.474a
		4.35	b		3.29	b
ADT	A	9.75	c-0.156a	A	2.08	b
		10.5	b		7.28	a-0.949c
		21.4	a+0.409c		∞	a+0.883c
C1-ADT	Λ_Y	3.00	c+0.024a	A	0.92	b
	(0, 0.358, 0)	6.21	a+0.055c		8.62	c+0.154a
		7.58	b		25.0	a+0.015c
C6-ADT	X	4.05	c+0.265a	Λ_Y	3.08	c+0.597a
		4.80	b	(0, 0.191, 0)	7.74	a-0.068c
		45.8	a-0.026c		66.7	b
C12-ADT	G and Z	1.43	a-0.091b	Y and T	3.27	b+0.206a
		2.10	b+0.315a		5.94	a-0.021b
		∞	c+0.270a +0.046b		∞	c+0.270a +0.046b
Ph-ADT	X	1.56	c+0.836a	Γ	1.29	a+0.455c
		2.97	c-0.124a		1.78	c-0.039a
		3.39	b		4.07	b

We recall that the effective mass not only depends on electronic coupling, but also on intermolecular distance. For instance, in a one-dimensional tight-binding model, the effective mass is given by[57]

$$m = \frac{\hbar^2}{2td^2} \quad (5)$$

Although the phenyl acenedithiophene crystals are not ideal one-dimensional systems, we can compare the effective mass components in different directions using eq 5 to try and provide a better understanding of the transport characteristics in these crystals. As discussed in the previous section, the overall electronic coupling for the interlayer pairs is about one tenth that for the intralayer pairs, while the interlayer distance is four times larger than the intermolecular distances for the intralayer pairs. Since the effective mass decreases linearly with electronic coupling and quadratically with intermolecular distance, the effective mass along the interlayer direction is reasonably similar to that within the molecular layer.

Despite the similar herringbone-type molecular layers in the unsubstituted NDT crystal, much larger effective masses are found along the interlayer direction. This can be attributed to the *ca.* twice smaller interlayer distance and to much larger angles between the direction along the molecular pairs and the interlayer direction (which substantially reduces the effective electronic coupling along the interlayer direction).

The decrease in effective mass for electrons along the π-stacking direction in going from ADT to C1-ADT (2.08 to 0.92 m_0) can also be rationalized by means of eq 5. The electronic

dx.doi.org/10.1021/jp210778w | J. Phys. Chem. C 2012, 116, 5215−5224

coupling for the molecular pair along the π-stacking direction increases by 25% from ADT to C1-ADT (108.9 to 135.8 meV), while there is a 43% increase of the intermolecular distance (4.01 to 5.73 Å); this leads to a 40% decrease in electron effective mass by use of eq 5. The latter value is in very good agreement with the result (decrease by 44%) obtained from the crystal band structure calculations.

Nonlocal Electron-Vibration Couplings. Electron−phonon (vibration) interactions play an important role in determining the charge-transport mechanism in molecular organic semiconductors. There are two major sources of electron−phonon interactions corresponding to local and nonlocal couplings.[38,58] The local coupling represents a key interaction in Holstein-type polaron models,[59,60] and its strength is reflected in the polaron binding energy, E_{pol}, or, in the context of Marcus electron-transfer theory, in the reorganization energy λ ($\approx 2E_{pol}$), which we discussed earlier. Here we focus on the nonlocal or so-called Peierls-type electron−phonon coupling,[61] which arises from the modulation of the transfer integrals by thermal vibrations of the molecules in the solid. The overall strength of this coupling can also be expressed by a microscopic parameter (L) that carries a physical meaning similar to λ.[62,63] In the high-temperature limit, it can be derived from the variance of the transfer integrals due to thermal fluctuations[62]

$$\sigma^2 = \langle (t - \langle t \rangle)^2 \rangle = 2Lk_BT \quad (6)$$

Here $\langle \cdots \rangle$ represents the statistical average over vibrational coordinates. The variance σ and the average $\langle t \rangle$ of the transfer integrals are obtained by a Gauss fitting of the probability distribution for the transfer integrals that can be derived as a time average by means of MD simulations.[49,64,65]

Since the spatial overlap between molecules in interlayer or interstack molecular pairs is vanishingly small, the transfer integrals hardly vary due to such intermolecular coordinate changes. As a result, the nonlocal coupling for such pairs can be expected to be very small. Therefore, because of the very large number of transfer integrals that need to be evaluated, we have chosen here to perform calculations only on molecular pairs A, that are representative of the intralayer or intrastack pairs. The standard deviations σ, values $\langle t \rangle$, and parameters L at room temperature are reported in Table 7 (there are noticeable differences between the transfer integrals shown in Tables 4 and 7 that can be attributed the differences in the DFT and COMPASS optimized crystal geometries). If we focus on the L parameters, moderate and similar L values for holes and electrons are found for all the herringbone-type pairs in the NDT, Ph-NDT, and Ph-ADT crystals, in the range of 5−12 meV; these values are similar to what is found for the herringbone pair in pentacene.[63] On the other hand, much larger L values are found for the π-stacking pairs in the ADT and C1-ADT crystals; especially, the L value for holes in the ADT crystal is as high as 135.5 meV.

Table 7. Standard Deviations σ, the Average Values $\langle t \rangle$, and Parameters L of the Transfer Integrals Estimated at Room Temperature (298 K) for Molecular Pairs A in the Studied NDT and ADT Crystals (All in meV)

	σ_h	$\langle t_h \rangle$	L_h	σ_e	$\langle t_e \rangle$	L_e
NDT	23.8	62.0	11.0	24.9	−48.9	12.0
C8-NDT	19.1	39.4	7.1	22.4	61.1	9.7
Ph-NDT	17.0	−3.3	5.6	19.8	−16.3	7.6
ADT	83.7	24.0	135.5	42.4	70.3	34.8
C1-ADT	46.7	8.3	42.2	40.8	110.6	32.2
C6-ADT	11.2	1.0	2.4	20.2	40.8	7.9
C12-ADT	37.1	97.7	26.6	23.0	−27.6	10.2
Ph-ADT	16.6	−9.1	5.3	16.3	−26.6	5.1

4. CONCLUSIONS

In summary, we have investigated the electronic structure and charge-transport parameters of NDT and ADT and their dialkyl and diphenyl derivatives at the molecular and crystal levels, by means of DFT and MD calculations. The results indicate that, with respect to the parent acenedithiophenes, alkyl substitutions lead to very similar geometry modifications upon both oxidation and reduction. As a consequence, the unsubstituted and dialkylated acenedithiophenes present similar reorganization energies, ca. 260 and 140 meV for hole transport and ca. 230 and 160 meV for electron transport in the NDT and ADT series, respectively. The geometry relaxations upon ionizations for the diphenyl derivatives reflect both bond-length changes in the central acenedithiophene core and torsion-angle modifications between the acenedithiophene core and the terminal phenyl groups. The reorganization energies for hole transport in the diphenyl NDT and ADT compounds are close to the values in the unsubstituted and dialkylated derivatives, 245 and 158 meV, respectively. This is consistent with small changes in torsion angles and similar bond-length modifications upon oxidation. On the other hand, the reorganization energies for electron transport are 338 meV in Ph-NDT and 239 meV in Ph-ADT, that is ca. 50% larger than in the unsubstituted and dialkylated NDT and ADT systems; this is due to substantial changes in torsion angles as well as some large bond-length modifications upon reduction.

The results of transfer integrals and effective masses point out that one-, two-, or three-dimensional transport can be achieved in these acenedithiophene crystals: (1) C8-NDT displays a one-dimensional hole transport along the stacks in the b direction while one-dimensional electron transport is expected to take place along the π-stack direction in the ADT and C1-ADT crystals; (2) two-dimensional transport for electrons [holes] would occur along the parallel-stacking molecular layers in the C8-NDT [C12-ADT] crystal and for both types of carriers along the herringbone plane in the NDT crystal; and (3) most interestingly, three-dimensional transport for both holes and electrons could be realized in the Ph-NDT and Ph-ADT crystals; in particular, it is predicted that charge carrier mobility could be very high along the direction perpendicular to the herringbone plane. The Ph-NDT and Ph-ADT crystals are also those that present the smallest electron-vibration coupling associated to thermal fluctuations of the electronic couplings for the molecular pairs with largest transfer integrals.

We hope that the results presented here will be of enough interest to stimulate the measurements of the transport properties, especially for the ADT derivatives.

■ ASSOCIATED CONTENT

Supporting Information

DFT-B3LYP/6-31G(d,p)-calculated bond-length changes in the central NDT and ADT cores upon oxidation/reduction of the NDT and ADT compounds (Figure S1); molecular geometries of the NDT and ADT derivatives taken from the experimental and DFT-optimized crystals (Figure S2); electronic band structures and density of states based on the

experimental crystal geometries (Figure S3); normalized probability distributions of the transfer integrals for holes and electrons in pairs A (Figures S4 and S5); crystallographic parameters for the unit cells of the NDT and ADT derivatives (Table S1); hole and electron transfer integrals for the molecular pairs taken from the experimental crystal structures (Table S2); and hole and electron effective masses at the band extrema based on the experimental crystal geometries (Table S3). This material is available free of charge via the Internet at http://pubs.acs.org.

AUTHOR INFORMATION

Corresponding Author

*E-mail: jean-luc.bredas@chemistry.gatech.edu.

Notes

The authors declare no competing financial interest.

[†]Also affiliated with the Department of Chemistry, King Abdulaziz University, Jeddah 21589, Saudi Arabia.

ACKNOWLEDGMENTS

The authors acknowledge many stimulating discussions with Dr. V. Coropceanu. This work has been supported in part by the MRSEC Program of the NSF (Award No. DMR-0819885) and the Office of Naval Research. The computational resources have been made partly available via the CRIF Program of the NSF (Award No. CHE-0946869).

REFERENCES

(1) Garnier, F.; Hajlaoui, R.; Yassar, A.; Srivastava, P. *Science* **1994**, *265*, 1684.
(2) Sirringhaus, H.; Tessler, N.; Friend, R. H. *Science* **1998**, *280*, 1741.
(3) Katz, H. E.; Lovinger, A. J.; Johnson, J.; Kloc, C.; Siegrist, T.; Li, W.; Lin, Y. Y.; Dodabalapur, A. *Nature* **2000**, *404*, 478.
(4) Burroughes, J. H.; Bradley, D. D. C.; Brown, A. R.; Marks, R. N.; Mackay, K.; Friend, R. H.; Burns, P. L.; Holmes, A. B. *Nature* **1990**, *347*, 539.
(5) Sheats, J. R.; Antoniadis, H.; Hueschen, M.; Leonard, W.; Miller, J.; Moon, R.; Roitman, D.; Stocking, A. *Science* **1996**, *273*, 884.
(6) Friend, R. H.; Gymer, R. W.; Holmes, A. B.; Burroughes, J. H.; Marks, R. N.; Taliani, C.; Bradley, D. D. C.; Dos Santos, D. A.; Brédas, J. L.; Logdlund, M.; Salaneck, W. R. *Nature* **1999**, *397*, 121.
(7) Sariciftci, N. S.; Smilowitz, L.; Heeger, A. J.; Wudl, F. *Science* **1992**, *258*, 1474.
(8) Halls, J. J. M.; Walsh, C. A.; Greenham, N. C.; Marseglia, E. A.; Friend, R. H.; Moratti, S. C.; Holmes, A. B. *Nature* **1995**, *376*, 498.
(9) Yu, G.; Gao, J.; Hummelen, J. C.; Wudl, F.; Heeger, A. J. *Science* **1995**, *270*, 1789.
(10) Laquindanum, J. G.; Katz, H. E.; Lovinger, A. J.; Dodabalapur, A. *Adv. Mater.* **1997**, *9*, 36.
(11) Laquindanum, J. G.; Katz, H. E.; Lovinger, A. J. *J. Am. Chem. Soc.* **1998**, *120*, 664.
(12) Kwon, O.; Coropceanu, V.; Gruhn, N. E.; Durivage, J. C.; Laquindanum, J. G.; Katz, H. E.; Cornil, J.; Brédas, J. L. *J. Chem. Phys.* **2004**, *120*, 8186.
(13) Takimiya, K.; Kunugi, Y.; Konda, Y.; Niihara, N.; Otsubo, T. *J. Am. Chem. Soc.* **2004**, *126*, 5084.
(14) Payne, M. M.; Parkin, S. R.; Anthony, J. E.; Kuo, C. C.; Jackson, T. N. *J. Am. Chem. Soc.* **2005**, *127*, 4986.
(15) Coropceanu, V.; Kwon, O.; Wex, B.; Kaafarani, B. R.; Gruhn, N. E.; Durivage, J. C.; Neckers, D. C.; Brédas, J. L. *Chem.-Eur. J* **2006**, *12*, 2073.
(16) Dickey, K. C.; Anthony, J. E.; Loo, Y. L. *Adv. Mater.* **2006**, *18*, 1721.
(17) Takimiya, K.; Kunugi, Y.; Ebata, H.; Otsubo, T. *Chem. Lett.* **2006**, *35*, 1200.
(18) Chen, M. C.; Kim, C.; Chen, S. Y.; Chiang, Y. J.; Chung, M. C.; Facchetti, A.; Marks, T. J. *J. Mater. Chem.* **2008**, *18*, 1029.
(19) Kashiki, T.; Miyazaki, E.; Takimiya, K. *Chem. Lett.* **2008**, *37*, 284.
(20) Kashiki, T.; Miyazaki, E.; Takimiya, K. *Chem. Lett.* **2009**, *38*, 568.
(21) Goetz, K. P.; Li, Z.; Ward, J. W.; Bougher, C.; Rivnay, J.; Smith, J.; Conrad, B. R.; Parkin, S. R.; Anthopoulos, T. D.; Salleo, A.; Anthony, J. E.; Jurchescu, O. D. *Adv. Mater.* **2011**, *23*, 3698.
(22) Shinamura, S.; Osaka, I.; Miyazaki, E.; Nakao, A.; Yamagishi, M.; Takeya, J.; Takimiya, K. *J. Am. Chem. Soc.* **2011**, *133*, 5024.
(23) Shinamura, S.; Miyazaki, E.; Takimiya, K. *J. Org. Chem.* **2010**, *75*, 1228.
(24) Pietrangelo, A.; MacLachlan, M. J.; Wolf, M. O.; Patrick, B. O. *Org. Lett.* **2007**, *9*, 3571.
(25) Pietrangelo, A.; Patrick, B. O.; MacLachlan, M. J.; Wolf, M. O. *J. Org. Chem.* **2009**, *74*, 4918.
(26) Lee, C. T.; Yang, W. T.; Parr, R. G. *Phys. Rev. B* **1988**, *37*, 785.
(27) Becke, A. D. *J. Chem. Phys.* **1993**, *98*, 5648.
(28) Hehre, W. J.; Ditchfield, R.; Pople, J. A. *J. Chem. Phys.* **1972**, *56*, 2257.
(29) Harihara, P. C.; Pople, J. A. *Theor. Chim. Acta* **1973**, *28*, 213.
(30) Francl, M. M.; Pietro, W. J.; Hehre, W. J.; Binkley, J. S.; Gordon, M. S.; Defrees, D. J.; Pople, J. A. *J. Chem. Phys.* **1982**, *77*, 3654.
(31) Frisch, M. J.; Trucks, G. W.; Schlegel, H. B.; Scuseria, G. E.; Robb, M. A.; Cheeseman, J. R.; Scalmani, G.; Barone, V.; Mennucci, B.; Petersson, G. A.; et al. *Gaussian 09*, revision A.02, Gaussian, Inc.: Wallingford, CT, 2009.
(32) Dovesi, R.; Saunders, V. R.; Roetti, C.; Orlando, R.; Zicovich-Wilson, C. M.; Pascale, F.; Civalleri, B.; Doll, K.; Harrison, N. M.; Bush, I. J.; et al.; University of Torino: Torino, Italy, 2006.
(33) Monkhorst, H. J.; Pack, J. D. *Phys. Rev. B* **1976**, *13*, 5188.
(34) Bunte, S. W.; Sun, H. *J. Phys. Chem. B* **2000**, *104*, 2477.
(35) Senthilkumar, K.; Grozema, F. C.; Bickelhaupt, F. M.; Siebbeles, L. D. A. *J. Chem. Phys.* **2003**, *119*, 9809.
(36) Valeev, E. F.; Coropceanu, V.; da Silva Filho, D. A.; Salman, S.; Brédas, J. L. *J. Am. Chem. Soc.* **2006**, *128*, 9882.
(37) Delgado, M. C. R.; Pigg, K. R.; Filho, D. A. d. S.; Gruhn, N. E.; Sakamoto, Y.; Suzuki, T.; Malave Osuna, R.; Casado, J.; Hernandez, V.; Lopez Navarrete, J. T.; et al. *J. Am. Chem. Soc.* **2009**, *131*, 1502.
(38) Coropceanu, V.; Cornil, J.; da Silva Filho, D. A.; Olivier, Y.; Silbey, R.; Brédas, J. L. *Chem. Rev.* **2007**, *107*, 926.
(39) Norton, J. E.; Brédas, J. L. *J. Am. Chem. Soc.* **2008**, *130*, 12377.
(40) McMahon, D. P.; Troisi, A. *J. Phys. Chem. Lett.* **2010**, *1*, 941.
(41) Malagoli, M.; Coropceanu, V.; da Silva, D. A.; Brédas, J. L. *J. Chem. Phys.* **2004**, *120*, 7490.
(42) Coropceanu, V.; Malagoli, M.; da Silva, D. A.; Gruhn, N. E.; Bill, T. G.; Brédas, J. L. *Phys. Rev. Lett.* **2002**, 89.
(43) da Silva, D. A.; Kim, E. G.; Brédas, J. L. *Adv. Mater.* **2005**, *17*, 1072.
(44) Chesterfield, R. J.; McKeen, J. C.; Newman, C. R.; Ewbank, P. C.; da Silva, D. A.; Brédas, J. L.; Miller, L. L.; Mann, K. R.; Frisbie, C. D. *J. Phys. Chem. B* **2004**, *108*, 19281.
(45) Brédas, J. L.; Calbert, J. P.; da Silva, D. A.; Cornil, J. *Proc. Natl. Acad. Sci. U.S.A.* **2002**, *99*, 5804.
(46) Pope, M.; Swenberg, C. E. *Electronic Processes in Organic Crystals and Polymers*; 2nd ed.; Oxford University Press: New York, 1999.
(47) Marcus, R. A. *Rev. Mod. Phys.* **1993**, *65*, 599.
(48) Barbara, P. F.; Meyer, T. J.; Ratner, M. A. *J. Phys. Chem.* **1996**, *100*, 13148.
(49) Martinelli, N. G.; Olivier, Y.; Athanasopoulos, S.; Ruiz Delgado, M.-C.; Pigg, K. R.; da Silva Filho, D. A.; Sánchez-Carrera, R. S.; Venuti, E.; Della Valle, R. G.; Brédas, J. L.; et al. *ChemPhysChem* **2009**, *10*, 2265.
(50) Wang, L.; Li, Q.; Shuai, Z.; Chen, L.; Shi, Q. *Phys. Chem. Chem. Phys.* **2010**, *12*, 3309.
(51) Stehr, V.; Pfister, J.; Fink, R. F.; Engels, B.; Deibel, C. *Phys. Rev. B* **2011**, *83*, 155208.

(52) Nan, G.; Wang, L.; Yang, X.; Shuai, Z.; Zhao, Y. *J. Chem. Phys.* **2009**, *130*, 024704.
(53) Nan, G.; Yang, X.; Wang, L.; Shuai, Z.; Zhao, Y. *Phys. Rev. B* **2009**, *79*, 115203.
(54) Di Motta, S.; Di Donato, E.; Negri, F.; Orlandi, G.; Fazzi, D.; Castiglioni, C. *J. Am. Chem. Soc.* **2009**, *131*, 6591.
(55) Seeger, K. *Semiconductor Physics: An Introduction*; 9th ed.; Springer-Verlag: Berlin, 2004.
(56) de Wijs, G. A.; Mattheus, C. C.; de Groot, R. A.; Palstra, T. T. M. *Synth. Met.* **2003**, *139*, 109.
(57) Kittel, C. *Quantum Theory of Solids*; Wiley: New York, 1963.
(58) Brédas, J. L.; Beljonne, D.; Coropceanu, V.; Cornil, J. *Chem. Rev.* **2004**, *104*, 4971.
(59) Holstein, T. *Ann. Phys.* **1959**, *8*, 343.
(60) Holstein, T. *Ann. Phys.* **1959**, *8*, 325.
(61) Peierls, R. E. *Quantum Theory of Solids*; Oxford University Press: New York, 2001.
(62) Coropceanu, V.; Sanchez-Carrera, R. S.; Paramonov, P.; Day, G. M.; Brédas, J. L. *J. Phys. Chem. C* **2009**, *113*, 4679.
(63) Sanchez-Carrera, R. S.; Paramonov, P.; Day, G. M.; Coropceanu, V.; Brédas, J. L. *J. Am. Chem. Soc.* **2010**, *132*, 14437.
(64) Troisi, A.; Orlandi, G. *J. Phys. Chem. A* **2006**, *110*, 4065.
(65) Zhu, L.; Kim, E. G.; Yi, Y.; Ahmed, E.; Jenekhe, S. A.; Coropceanu, V.; Brédas, J. L. *J. Phys. Chem. C* **2010**, *114*, 20401.